DEAR Technical Note IR-2

Summary of Foil Measurements, Foil Monte Carlo, and Recommendations for the Long Term Calibration

Takeyasu M. Ito

Laboratori Nazionali di Frascati
I.N.F.N., Frascati, Italy

Ross King

Institute for Medium Energy Physics
Austrian Academy of Sciences, Vienna, Austria

June 6, 1998

1 Introduction

The long term calibration will utilize characteristic X rays emitted from thin metal foils placed either on the inner wall of the target cell, or below the entrance window of the target cell (or both). The metal foils are excited either by incoming slow kaons, or by background radiation (or both). Titanium and zirconium will be used as foil materials, so that their characteristic X-ray peaks (titanium: 4.5 keV; zirconium: 15.8 keV) fall below and above the region of interest.

A series of so called "foil measurements" were performed to have an idea of what would be the optimum configuration of the foils for the long term calibration. In addition, a Monte Carlo was created and run in order to understand the experimental results and to extrapolate these results to a realistic background excitation spectrum.

In order to determine the optimum configuration of the foil arrangement, we concentrated on the following points in the experiments and Monte Carlo:

1. Intensity ratio of titanium and zirconium K_α X rays as detected by CCD's (and analyzed using the single pixel method) for the identical configuration (the same area of foils at the same position, the same source for excitation, etc.). The difference between titanium and zirconium mainly arises from the different excitation cross section and the different detection efficiency of the CCD for X rays of different energy.

Table 1: X rays emitted by an ^{241}Am source [1]. The first five entries arise from Np L-series X rays. The average energy and total yield for a given series is listed.

X-ray energy	Intensity (%)
11.87	0.86
13.90	13.0
15.86	0.37
17.54	18.4
22.0	4.7
26.4	2.4
59.5	35.7

to the K-edge of zirconium, and in the latter case because of the high intensity of the line. The fact that the sources of excitation are different for titanium and zirconium introduces a certain complexity in the interpretation of the results, which requires a Monte Carlo calculation for a complete understanding.

Measurements were performed under the condition listed in table 2. For measurements 1-6, the bottom foil was placed at position 1, for an easier handling of the equipment. However, for measurements 8, the bottom foil was placed at position 2 in order to see the effect of the bottom foil in a more realistic configuration.

3 Results of the Measurement

The obtained spectra are shown in figures 2 - 9. For each of these spectra, the ordinate is in the unit of the channel of ADC and every four channel is packed into one bin.

The number of counts in each peak (titanium K_α and zirconium K_α) in each spectrum was obtained by fitting the spectra with a Gaussian function plus a linear background. The results are summarized in tables 3 and 4. In table 4, the average over all the CCD's used are shown with the conditions under which the data is taken, whereas in table 3, results from the individual CCD's are shown.

From table 3, it can be seen that the number of counts in the zirconium peak sometimes varies considerably from CCD to CCD. This is partly because the zirconium K_α peak is too close to the edge of the spectrum (the upper limit of the ADC range) and sometimes zirconium K_α X-ray signal may become an overflow depending on the noise level. Indeed sometimes the zirconium peak is indistinguishable from the overflow peak (see e.g. figure 7, CCD 1). Therefore, in interpreting the results, the number of counts in the zirconium peak should be understood to have an error larger than that given simply by the statistics.

It can also be seen in this table that the number of counts in the titanium peak

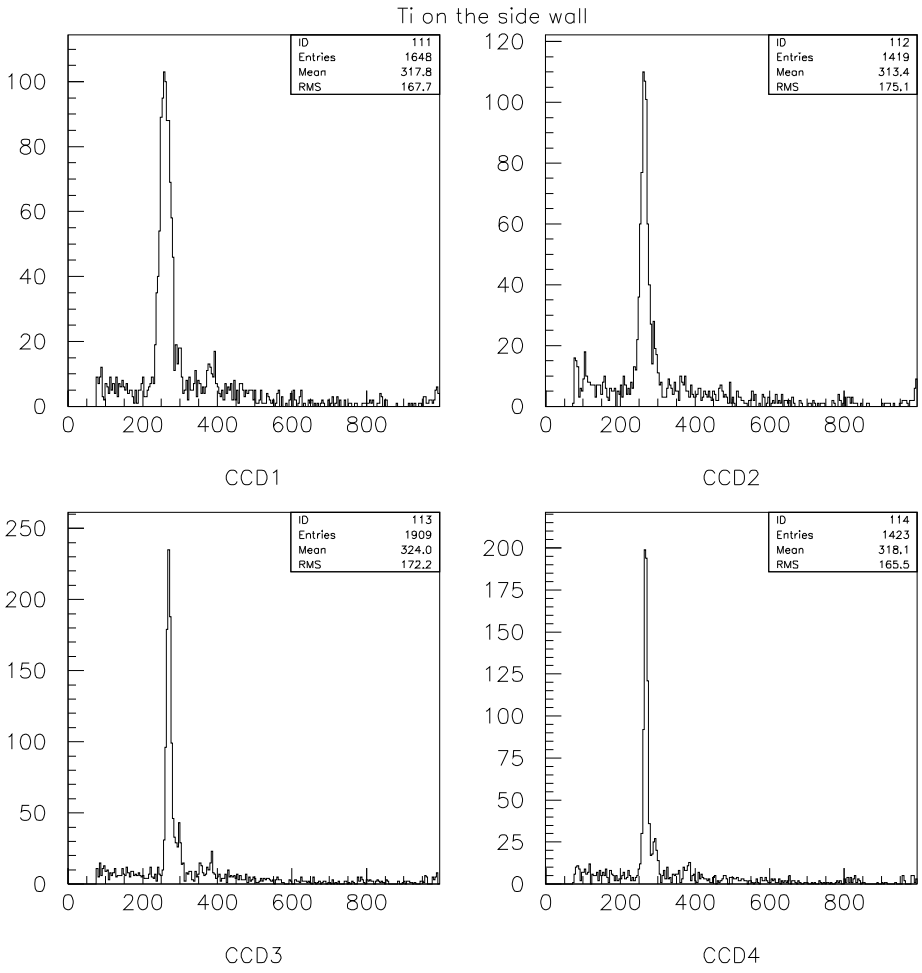

Figure 2: X-ray spectra obtained from a measurement with titanium foils on the side wall, experimental configuration 1.

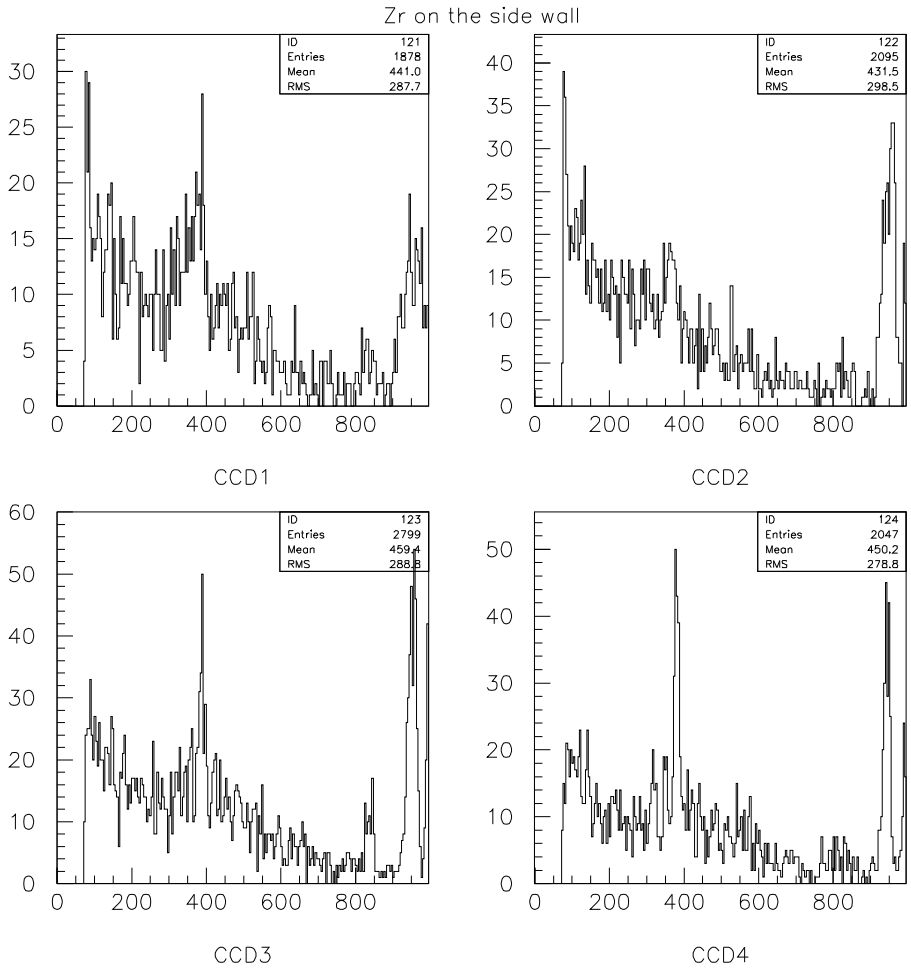

Figure 3: X-ray spectra obtained from a measurement with zirconium foils on the side wall. We see some iron X rays in the spectra. These iron X rays are from the stainless steel ring used as the spacer to hold the target cell, experimental configuration 2.

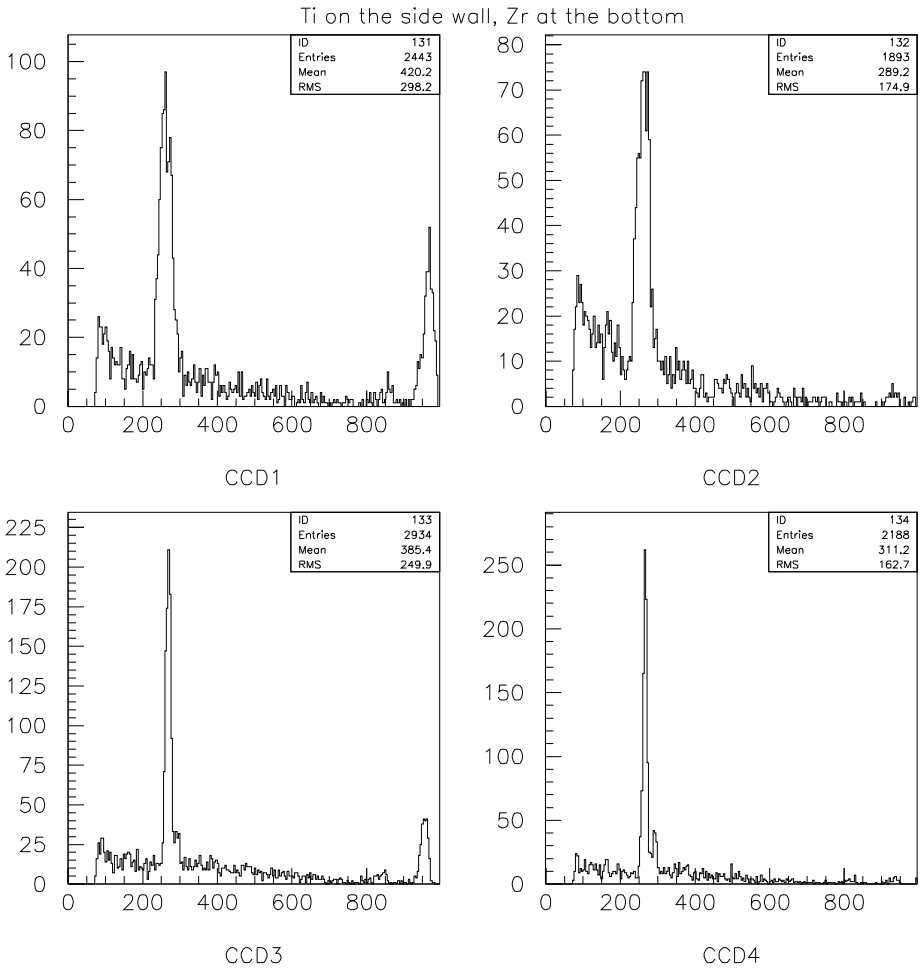

Figure 4: X-ray spectra obtained from a measurement with titanium foils on the side wall and zirconium foils at the bottom, experimental configuration 3.

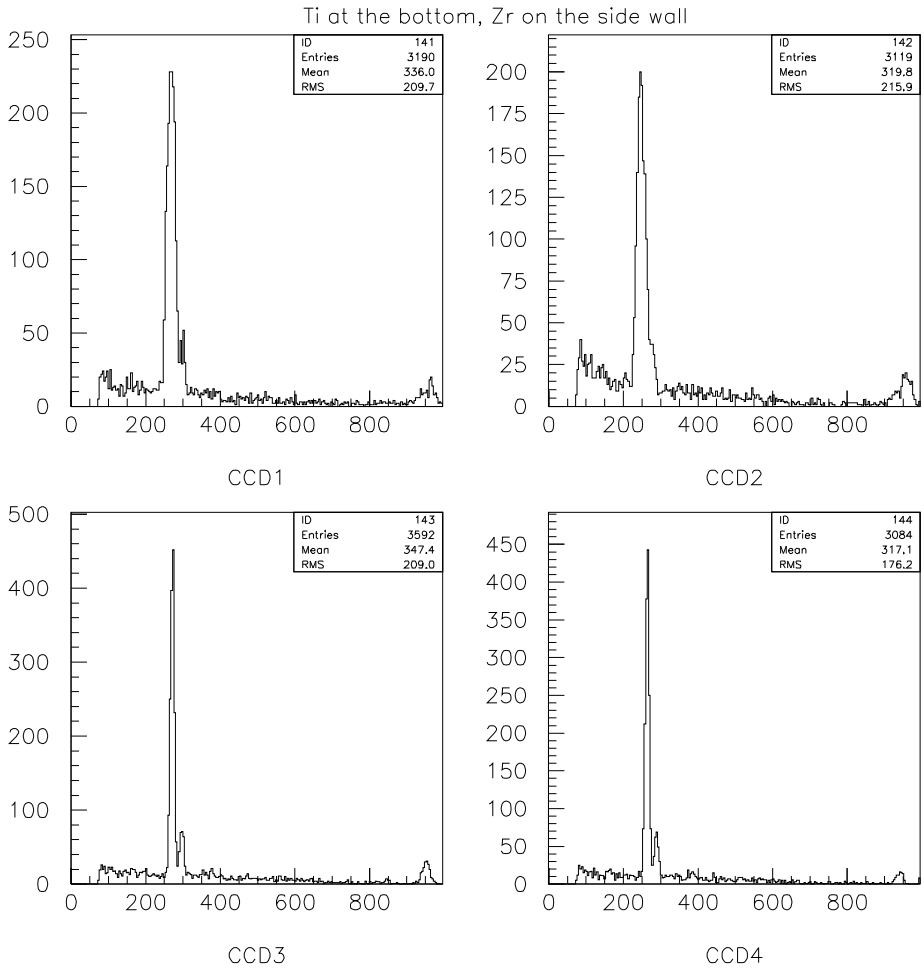

Figure 5: X-ray spectra obtained from a measurement with titanium foils at the bottom and zirconium foils on the side wall, experimental configuration 4.

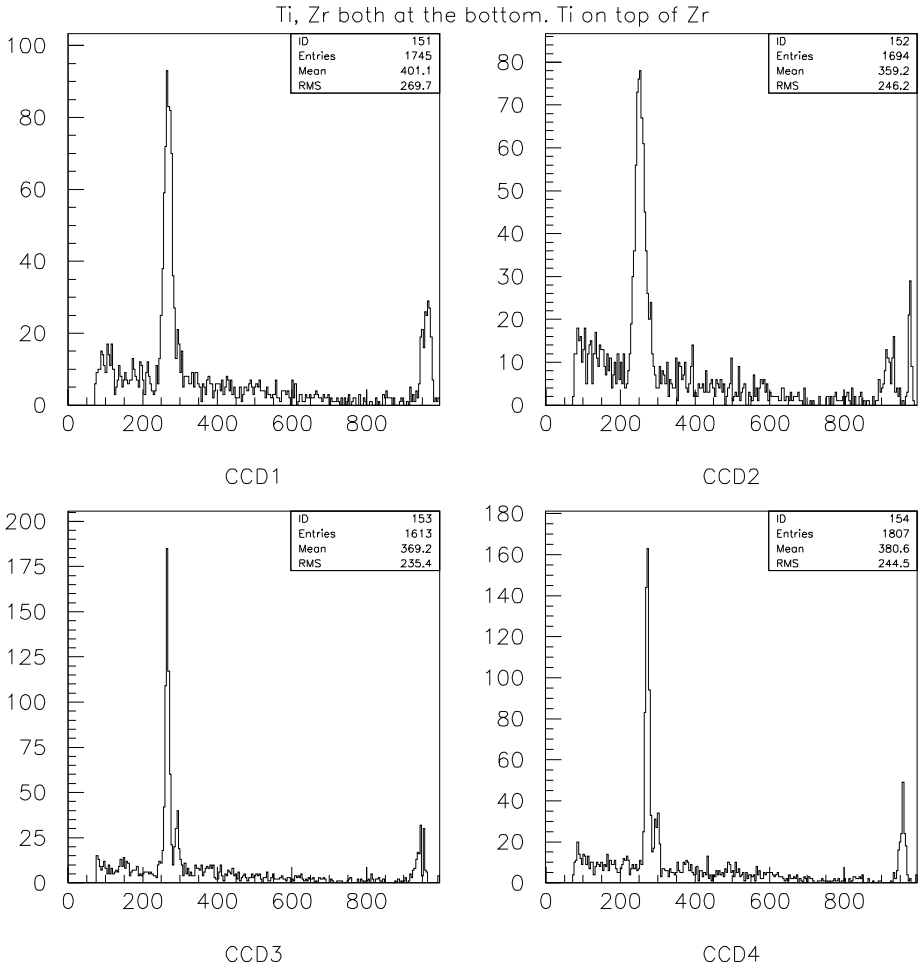

Figure 6: X-ray spectra obtained from a measurement with both titanium and zirconium foils at the bottom. The titanium foil was on the top of the zirconium foil, experimental configuration 5.

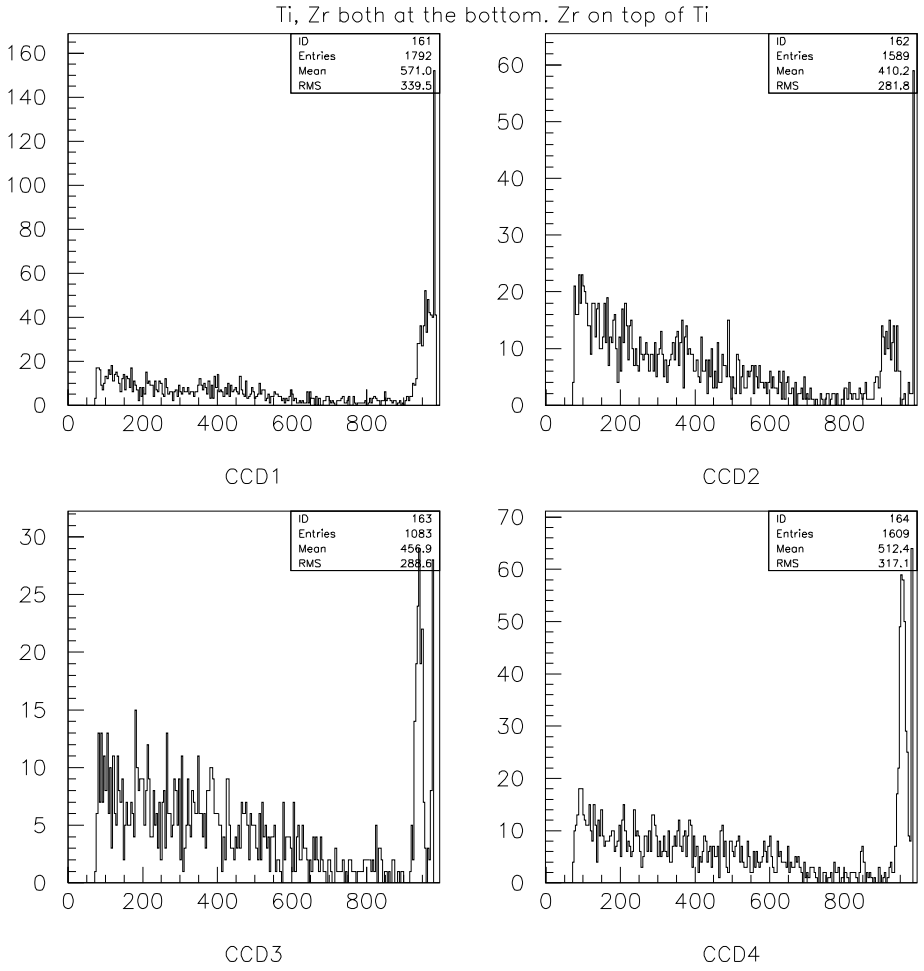

Figure 7: X-ray spectra obtained from a measurement with both titanium and zirconium foils at the bottom. The zirconium foil was on the top of the titanium foil, experimental configuration 6.

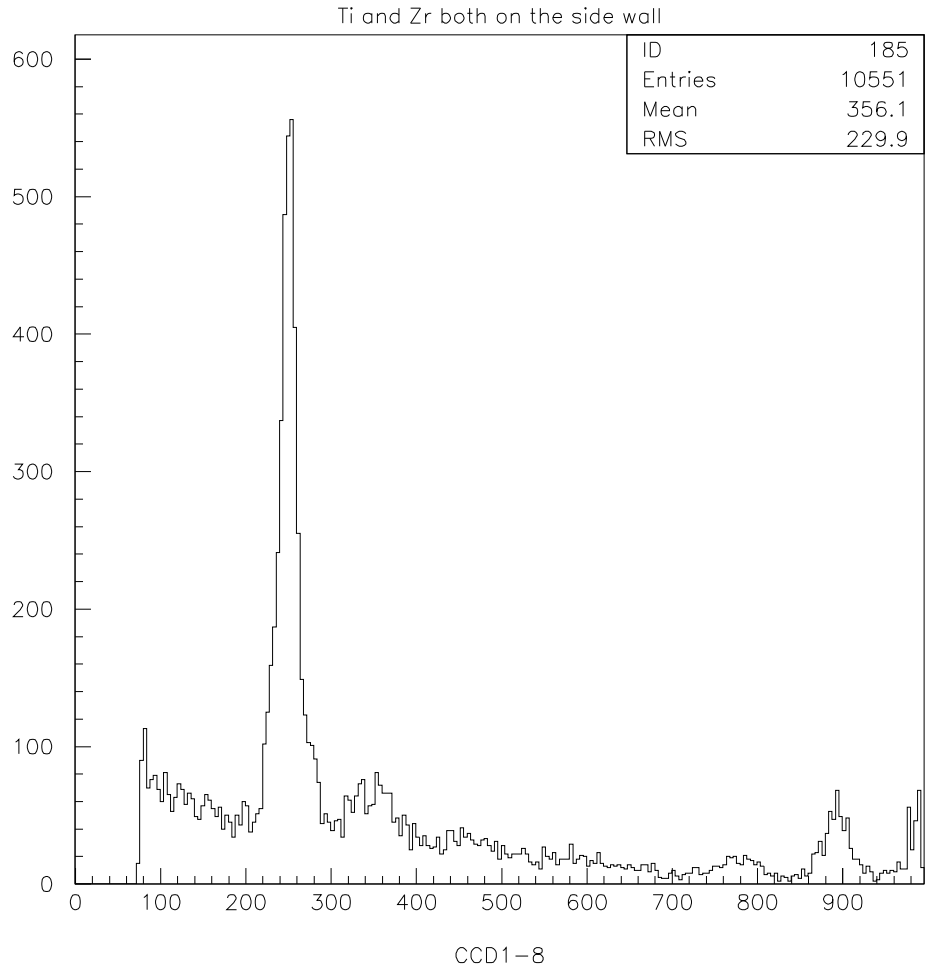

Figure 8: X-ray spectra obtained from a measurement with both titanium and zirconium foils on the side wall. Two of the corners in the inner wall of the target cell were covered with titanium foils and the other two were covered with zirconium foils. In addition to the Ti and Zr X rays, manganese K X rays (for this measurement an ^{55}Fe source was placed in the vacuum jacket and shielded by a piece of lead but the shielding was not complete) and neptunium L X rays (from the ^{241}Am source) can be seen in the spectrum, experimental configuration 7.

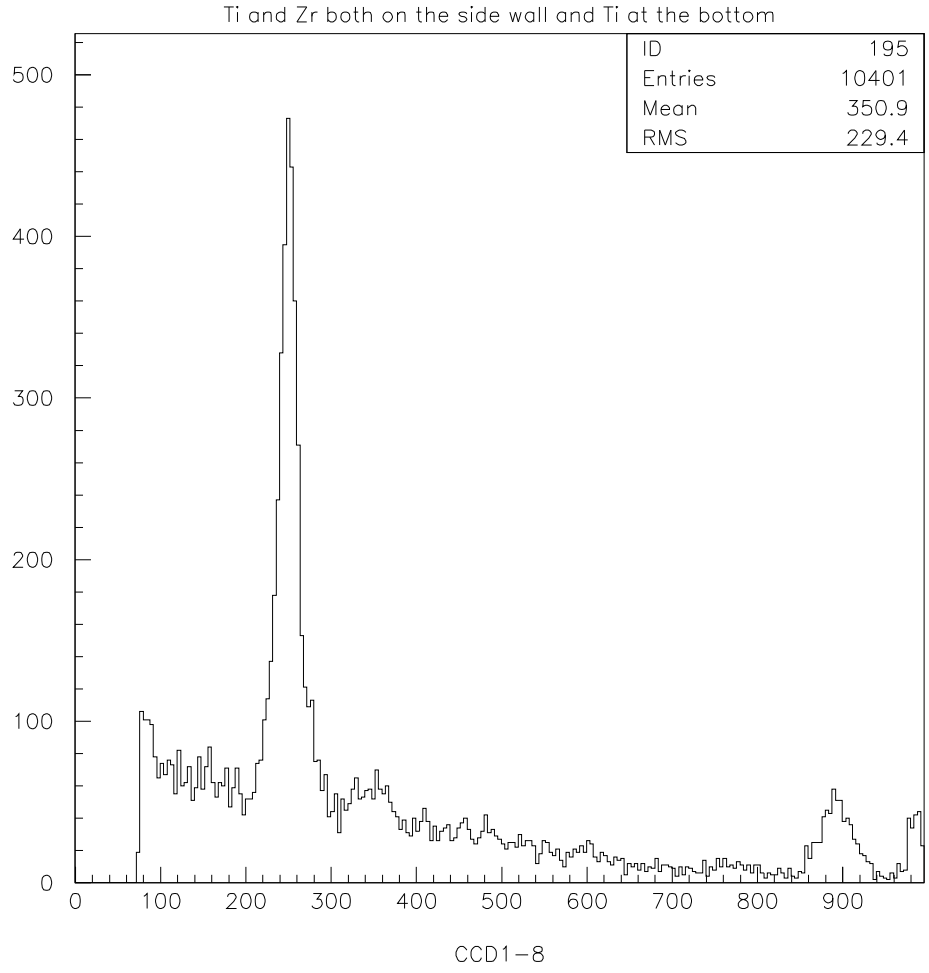

Figure 9: X-ray spectra obtained from a measurement with both titanium and zirconium foils on the side wall and a titanium foil at the bottom. Two of the corners in the inner wall of the target cell were covered with titanium foils and the other two were covered with zirconium foils. In addition to the Ti and Zr X rays, manganese K X rays (for this measurement an ^{55}Fe source was placed in the vacuum jacket and shielded by a piece of lead but the shielding was not complete) and neptunium L X rays (from the ^{241}Am source) can be seen in the spectrum, experimental configuration 8.

varies somewhat from CCD to CCD. This effect can at least be partially explained by geometry, and is discussed in section 4.

4 The Monte Carlo

There were several reasons to investigate foil excitations through a Monte Carlo simulation. First, the spectrum of ^{241}Am is complex, which hinders simple hand calculations. Second, geometrical effects, such as CCD acceptance, shadowing, and effective foil thickness are significant. Finally, we were interested in calculating the effects of secondary excitation (Ti K_α X rays excited by Zr K_α X rays), and the expected signal ratios excited by a realistic background spectrum and by kaons.

4.1 The Algorithm

A simulation using the following algorithm was created:

1. Read photoelectric cross section data
2. Read the description of the geometry
3. Generate a photon from a given distribution:
   if the desired number has been generated, stop the process
4. Propagate the photon:
   if an interaction occurs, go to step 5
   if the photon leaves the volume go to step 3
5. Check the interaction:
   if the particle is absorbed, go to step 3
   if an X ray is excited, reset the energy and direction, go to step 4

Step 5 is crucial. It is not only necessary to take into account the fluorescent yields of the K-shells given in table 8, but also to note the probability of a K-shell excitation for a given interaction [4]. This probability is approximated by the ratio of the photoelectric cross sections immediately above and below the K-edge of the material, and the values are 0.878 for titanium and 0.841 for zirconium.

4.2 Single-Pixel Analysis Efficiency

In addition to accounting for the CCD efficiency as a function of energy, it is also necessary to account for the analysis efficiency as a function of energy. It has so far been assumed that the single-pixle analysis is 100% effecient. A check of the online analysis indicates that this is far from the case - refer to table 6.

Assuming that the final values in table 6 are the true numbers of single-pixel X rays, we conclude that for the normal 2-sigma cuts, which are the default for the

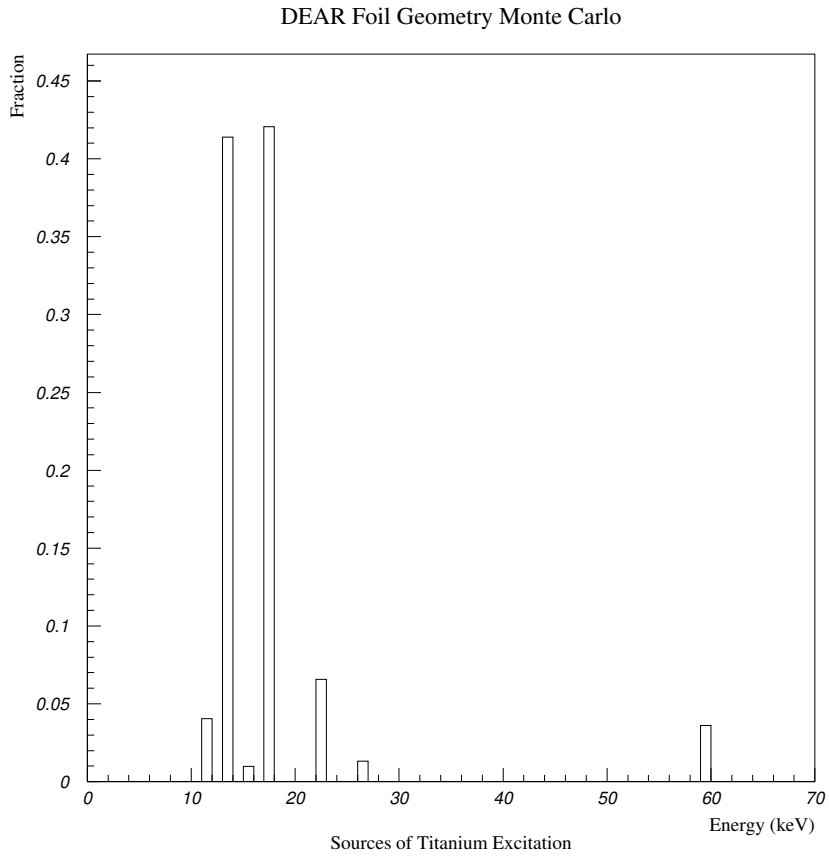

Figure 10: A Monte Carlo spectrum of ^{241}Am photons that excited titanium K-series X rays, which were in turn detected in the CCDs.

online analysis (and were used for the data shown in this report), the efficiency in the region of 5 keV is 90%, and in the region of 15 keV is only 60%!

The more advanced IGOR analysis of D. Chatellard should avoid this energy-dependent effect. However, the actual efficiency of the final analysis is at this time unknown; 90% may be taken as a lower bound. In any case, users of the online analysis should be aware of this effect.

4.3 Some Monte Carlo Results

Important results are given in figures 10 and 11, which show the distribution of ^{241}Am X rays which excite K_α X rays detected in the CCDs for titanium and zirconium.

Some additional interesting observations were made during the course of the simulations. First, the observed number of counts is a strong function of geometry. In the case of wall foils, the X rays are generated preferentially near the bottom of

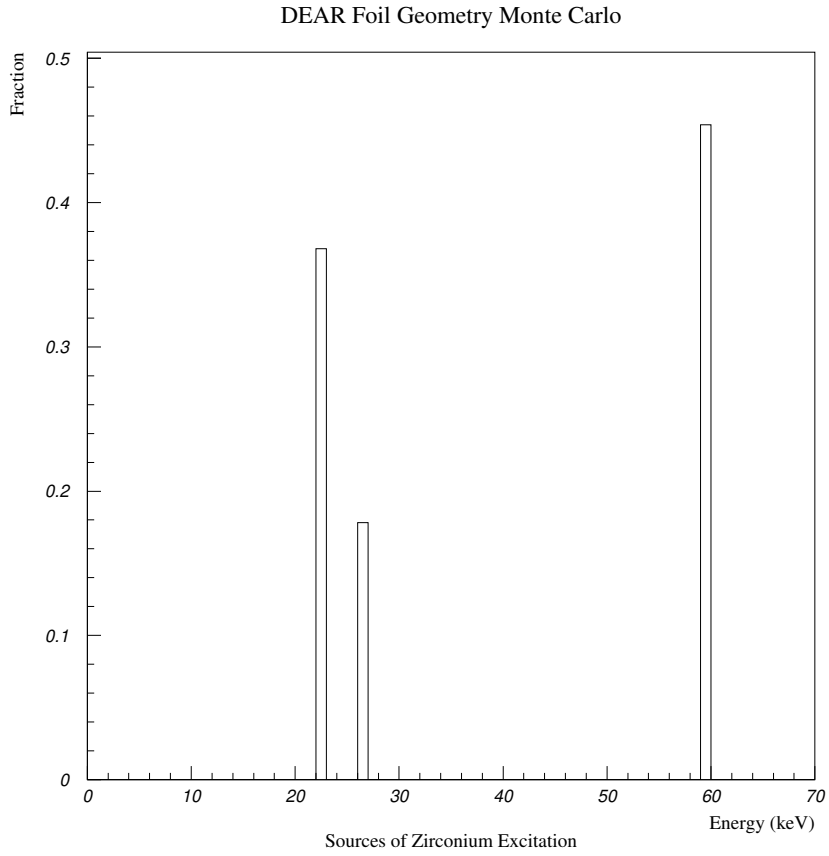

Figure 11: A Monte Carlo spectrum of ^{241}Am photons that excited zirconium K-series X rays, which were in turn detected in the CCDs.

the foils (this is a result of the decreasing solid angle intercepted by the foils as a function of height). Therefore, for wall foils or bottom foils, the vertical alignement of the CCDs is critical. If the CCDs are 5 mm too low, the count rate is reduced for both sources. If the CCDs are 5 mm too high, the count rate from the bottom foils is increased relative to that from wall foils. Furthermore, the horizontal alignment of the CCDs can affect the relative intensities from the various wall foils. This is due to the shadowing effect of the central bar of the target window frame. This same shadowing effect partially explains the differences in rates observed in two halves of the same chip, as seen in table 3.

The Monte Carlo results for each experimental arrangement are listed in table 5. These results will be discussed and compared with observations in section 5.

The Monte Carlo results for a realistic, continuous background spectrum will be discussed in section 7.

The Monte Carlo results for kaon excitation of the foils will be discussed in section 8.

5 Interpretation of the Measurements

In order to roughly understand the results quantitatively, the attenuation lengths of X rays of relevant energies in various materials are necessary. In table 7, the attenuation length for various X rays in titanium, zirconium, and mylar are listed.

From table 7, it can be seen that we can safely neglect the attenuation of the 13.9 keV and 18.6 keV X rays from the ^{241}Am source in the mylar windows, whose total thickness is 360 μm (see figure 1).

5.1 Consistency of the Data

It must be noted that the experimental data is not in itself consistent within the statistical errors.

For example, the number of Ti X rays observed in measurement 7 should be exactly half the number observed in measurement 1. Furthermore, the number of Zr X rays observed in measurement 6 should be smaller than the number observed in measurement 3.

Such discrepancies are likely the results of two significant systematic effects. First, as mentioned previously, the zirconium peak was very close to the overflow peak of the CCD spectra for some measurements. Second, the observed rates are a strong function of the CCD alignment, which was likly not always well reproduced between measurements.

For the above reasons, we must assume a large systematic error with respect to the experimental data. The Monte Carlo, on the other hand, is limited statistically, in that it requires more than two hours of CPU time to produce one hour of data. With this points in mind, one can see that the Monte Carlo reproduces the data

fairly well, in terms of absolute rate and in terms of relative rates for various foil geometries. We will elaborate on this theme in the following sections.

5.2 Expected Ti/Zr ratio for the identical geometry

The ratio of observed intensities of the titanium K_α X rays and zirconium K_α X rays can be obtained either by comparing the results of measurements 1 and 2 or from measurement 7. The ratio is:

$$\text{Measurement } 1/2: \quad \text{Ti/Zr} \simeq 5.7$$

$$\text{Measurement } 7: \quad \text{Ti/Zr} \simeq 6.3$$

From the Monte Carlo we have:

$$\text{Simulation } 1/2: \quad \text{Ti/Zr} \simeq 6.1$$

$$\text{Simulation } 7: \quad \text{Ti/Zr} \simeq 5.1$$

In this case, the first Monte Carlo result may be preferred over the second, due to better statistics in simulations 1 and 2.

How can we understand these results? As was mentioned earlier, there are two X-ray lines that contribute to the excitation of the titanium foils and two X-ray lines that contribute to the excitation of the zirconium foils. In order to compare the titanium and zirconium X-ray intensities for the identical configuration, it must be observed from table 7 that titanium K X rays will come only from the thin layer (20 μm) near the surface of the foil. Thus, only the flux of X rays absorbed in this thin layer can contribute to the generatation of titanium characteristic X rays that are observable (in this X-ray energy range, absorption is almost 100% due to the photoelectric effect, and also if kinematically possible, the photoelectric effect dominantly occurs with a K-shell electron). Therefore (referring to tables 8 and 7) the expected observed ratio is approximately:

$$\frac{[13 \times (1 - \exp(-\frac{20}{49.6})) + 18.4 \times (1 - \exp(-\frac{20}{95.6}))] \times \epsilon_{Ti}}{[35.7 \times (1 - \exp(-\frac{50}{402})) + 4.74 \times (1 - \exp(-\frac{50}{27.2}))] \times \epsilon_{Zr}} \simeq 6.5$$

where

$$\epsilon_{Ti} = 0.88 \times 0.192 \times 0.90 \times 0.83 \times 0.91 = 0.115$$

and

$$\epsilon_{Zr} = 0.84 \times 0.624 \times 0.99 \times 0.056 \times 0.58 = 0.017$$

In the efficiency formulae above, the first term is the probability of a K-shell excitation, the second term is the probability of a K_α excitation given a K-shell excitation, the third term is the target window transmission efficiency at the appropriate K_α energy, the fourth term is the CCD efficiency at the appropriate K_α energy, and

the final term is the efficiency of the online single-pixel analysis at the appropriate energy.

This back-of-the-envelope calculation contains all of the essential physics. The difference between this number (6.5) and the Monte Carlo result (6.0) is the result of geometry; mainly, that the excitation X rays pass through the mylar windows at sufficiently high angles to differentially attenuate the lower energy (titanium-exciting) and higher energy (zirconium-exciting) photons.

5.3 Zr foil at the bottom

By comparing measurements 1 and 3 or measurements 4 and 5, we can see that the titanium X-ray intensity is reduced by about a factor of two due to the presence of a zirconium foil at the bottom. Referring to table 7 and figure 10, the expected reduction in titanium X-ray intensity is:

$$1 - \frac{0.4 \times \exp(-\frac{50}{53.6}) + 0.4 \times \exp(-\frac{50}{17.9})}{0.4 + 0.4} = 48\%$$

The simulated titanium intensities are consistent with this simple calculation.

5.4 Ti foil at the bottom

By comparing measurements 2 and 4, it can be seen that the zirconium X-ray intensity reduces by 45% due to the presence of a titanium foil at the bottom. The same reduction should be seen between measurements 7 and 8, which is one of the major inconsistencies in the data that has already been mentioned.

Referring to table 7 and figure 11, we can again estimate:

$$1 - \frac{0.55 \times \exp(-\frac{50}{183}) + 0.45 \times \exp(-\frac{50}{2820})}{0.55 + 0.45} = 15\%$$

This is consistent with the Monte Carlo, which predicts 15%. Unfortunately, the measurements are untrustworthy, due to the large systematic effects already mentioned.

5.5 Ti foil on top of Zr foil

By comparing measurements 3 and 5, the effect of a titanium foil placed on top of a zirconium foil can be deduced. It can be seen that the intensity of the zirconium X ray is reduced by 40%. On the other hand, from table 7, the intensity of the 15.8 keV X ray is expected to be reduced in a 50 μm titanium foil by

$$1 - \exp(-\frac{50}{76.6}) = 51\%$$

which could be said to be consistent with the observation.

The most realistic number is probably given by simulations 3 and 5, which predict a reduction of 68%. The difference between this number and the estimate above can be attributed to the fact that zirconium X rays that hit the CCDs must pass through the titanium at a fairly large angle, thus increasing the effective thickness of the foil.

5.6 Zr foil on top of Ti foil

There are no titanium X rays observed when a zirconium foil is placed on top of a titanium foil (measurement 6). This is to be expected since the attenuation length of the 4.5 keV X ray in zirconium is only 2.5 μm.

5.7 Ti foil at the vacuum entrance

There are several arguments for having a foil at the vacuum entrance window. First, incoming slow kaons can serve very effectively to excite the foil and make a large contribution towards the generation of calibration X rays. Also, entrance foils have the potential to be a better source of calibration X rays excited by photon backgrounds as well, simply because all entering photons are incident on such a foil, whereas only a small percentage are incident on a given wall foils. And finally, it is expected that it will shield our detector from low energy (below 10 keV) X-ray background.

The argument against a foil at the vacuum entrance it is that the "good" background X rays that can excite the foils on the wall mainly come through the entrance window and the foil at the bottom may stop all these good X rays. Measurements 7 and 8 were carried out in order to test this possibility. To make the setup more realistic the bottom foil was placed at the position 2 (see figure 1).

Using the target cell in question, the CCDs have no acceptance for X rays originating from this position. Thus, with respect to zirconium, measurements 7 and 8 are a repeat of measurements 2 and 4. In this case, a reduction of 10% is observed, which is much closer to the prediction of section 5.4.

In terms of titanium, measurements 7 and 8 answer a new question, namely, what is the reduction of titanium K_α when the excitation X rays are shielded by titainium? By noting the attenuation lengths of 13.9 and 17.5 keV X rays in titanium, we can estimate:

$$1 - \frac{0.4 \times \exp(-\frac{50}{49.6}) + 0.4 \times \exp(-\frac{50}{95.6})}{0.4 + 0.4} = 52\%$$

This is an overestimate of the reduction because it neglects higher-energy excitation X rays (at 22 and 60 keV) that are less attenuated in titanium. Thus we have reasonable agreement with the observations (32%) and the simulations (45%).

and

$$\sigma_{\mathrm{Zr}} = \frac{\sigma_{\mathrm{CCD}}(16\ \mathrm{keV})}{\sqrt{N_{\mathrm{Zr}}}}$$

where N_{Ti} and N_{Zr} are the numbers of counts in the titanium and zirconium X-ray peaks, respectively. $\sigma_{\mathrm{CCD}}(4.5\ \mathrm{keV})$ and $\sigma_{\mathrm{CCD}}(16\ \mathrm{keV})$ are the energy resolution of the CCD detectors at 4.5 keV and 16 keV and it is estimated that

$$\sigma_{\mathrm{CCD}}(4.5\ \mathrm{keV}) = 160\ \mathrm{eV}$$

and

$$\sigma_{\mathrm{CCD}}(16\ \mathrm{keV}) = 230\ \mathrm{eV}.$$

Calculating the optimum Ti/Zr intensity ratio of the calibration peak yields,

$$\frac{N_{\mathrm{Ti}}}{N_{\mathrm{Zr}}} = \left(\frac{9.5}{2}\frac{160}{230}\right)^2 = 11.$$

7 Monte Carlo with a Realistic Background

The comparisons between observations, simple calculations, and the Monte Carlo results discussed in section 5 give us confidence in an extrapolation of the Monte Carlo with more more realistic, continuous background spectrum.

A photon spectrum generated by the DEAR background Monte Carlo was supplied by M. Bragadireanu and C. Petrascu. This spectrum was fit by a Gaussian in the region from 0 to 100 keV, as shown in figure 13. This Gaussian was then used as a new generator for the foil Monte Carlo.

Our test geometry consisted of two foils placed at position 2 (refer to figure 1) - a 75 micron titanium foil on top of a 25 micron zirconium foil - as well as the usual 50 micron titanium and zirconium foils on the target walls (as in experimental arrangement 7).

We reason that wall foils can only help. Meanwhile, an ^{55}Fe source will be inserted between the vacuum entrance window and the target entrance window. The target has been re-designed so that the CCDs have a large acceptance of X rays from this source. However, this means that the CCDs now have a larger acceptance for background X rays coming from beneath the table, a source that practically cannot be shielded. Therefore, it is desirable to have entrance foils that partially shield this background. Such foils should not block the ^{55}Fe calibration X rays, and yet be as close to the target as possible; thus, we choose the vaccum entrance window, even with the top of the table, just below the daily calibration source position.

We note that this foil combination makes a fairly decent filter below 10 keV. The transmission efficiency, convoluted with the CCD detection efficiency, is shown in figure 14. The problem is, zirconium becomes somewhat more transparent at energies just below the K-edge. We might want to consider adding another 25 microns of some higher-Z material (silver?) just before the zirconium layer to alleviate this problem.

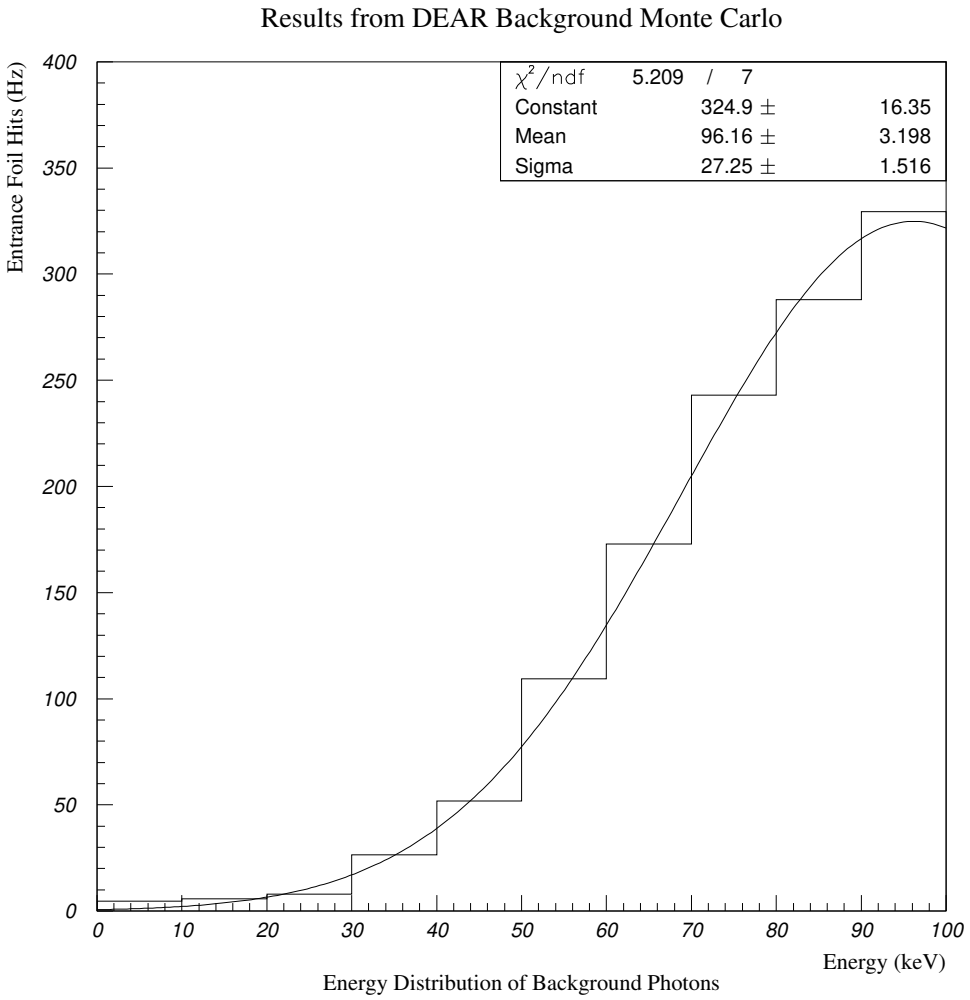

Figure 13: The energy spectrum of background photons incident on the entrance foils predicted by the DEAR background Monte Carlo, and a Gaussian fit.

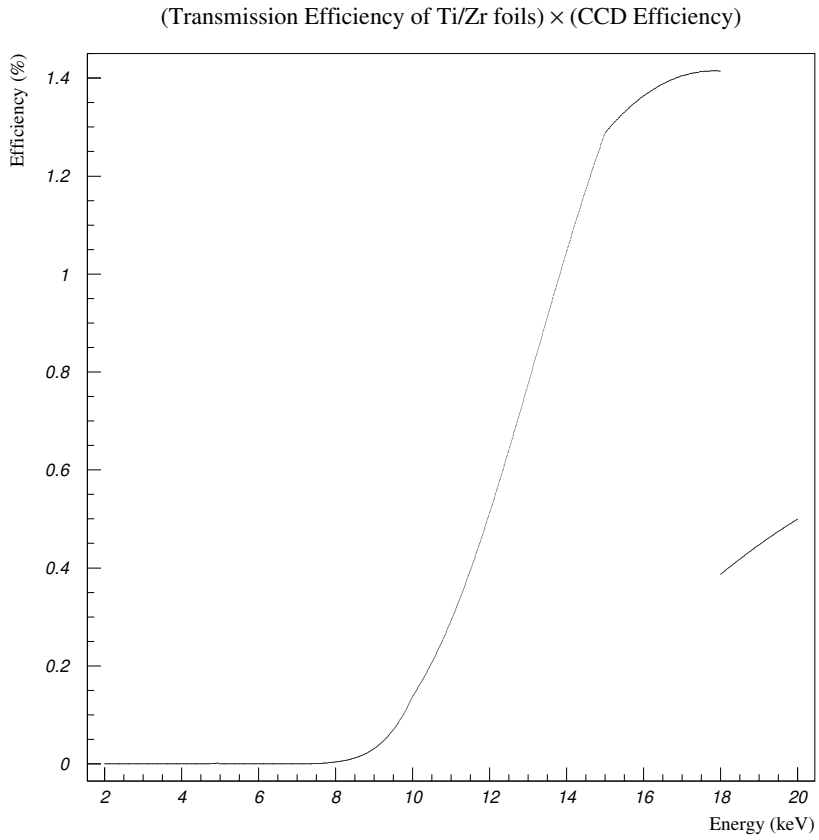

Figure 14: The transmission efficiency times the CCD detection efficiency of the 75 micron Ti / 25 micron Zr foil combination.

The equivalent of three days of background flux was generated. The K_α rates predicted by this simulation are as follows: for titanium, 275 events per day from the entrance foil, and 25 events per day from the wall foils. For zirconium, 140 events per day from the entrance foil, and 75 events per day from the wall foils.

8 Monte Carlo with Kaons

We were also interested in a more quantitative calculation of the number of calibration peak X rays excited by kaons.

The K-shell ionization cross section data for titanium was taken from reference [2] and fit with a third-order polynomial. The data is for protons, but the cross section is strictly a function of the velocity β, independent of the type of charged particle [3]. This means that calibration X rays will be excited equally by K^+ and K^- in the DEAR experiment. The data and fit results are shown in figure 15.

The momentum distributions of kaons incident on the calibration foils were created using a GEANT simulation of the DEAR geometry (including beam pipe, degrader, and entrance windows). These distributions were then used as inputs for the foil Monte Carlo. We considered the effect of kaons on titanium foils placed at the vacuum chamber entrance and on the target walls.

The results were as follows: for 500 pb^{-1} of data (about 10^9 kaon pairs generated), approximately 8500 titanium K_α X rays originating from kaon/anti-kaon excitation will be detected in the CCDs. Of these, about 75% originate from the bottom foil, and 25% from the wall foils.

With the same integrated luminosity, we expect to detect 10000 kaonic hydrogen K_α X rays, assuming a K_α yield of 1.5%. Thus, we estimate a ratio of 0.85:1 for calibration X rays excited by kaons alone. If we assume an instantaneous luminosity of 10 pb^{-1}/day, we expect about 200 kaonic hydrogen K_α X rays per day, and 170 titanium K_α X rays per day.

The case of zirconium was not simulated. However, the K-shell ionization cross section is roughly proportional to Z^{-4}. Thus we expect approximately one-tenth the number of titanium X rays to be excited, and about 6% of this number to be detected (compared to 85% for titanium). In other words, the excitation of zirconium by kaons will be neglibible compared to the excitation of titanium by kaons.

9 Summary and Recommendations

We first performed a series of so-called "foil measurements" aimed at finding the optimal arrangement of calibration foils. However, it quickly became clear that these measurements suffered from large systematic effects. We also realized that such measurements would be of limited use for extracting the expected calibration X ray rates under actual running conditions, due to the completely different excitation spectrum from the ^{241}Am source, compared to the true excitation sources.

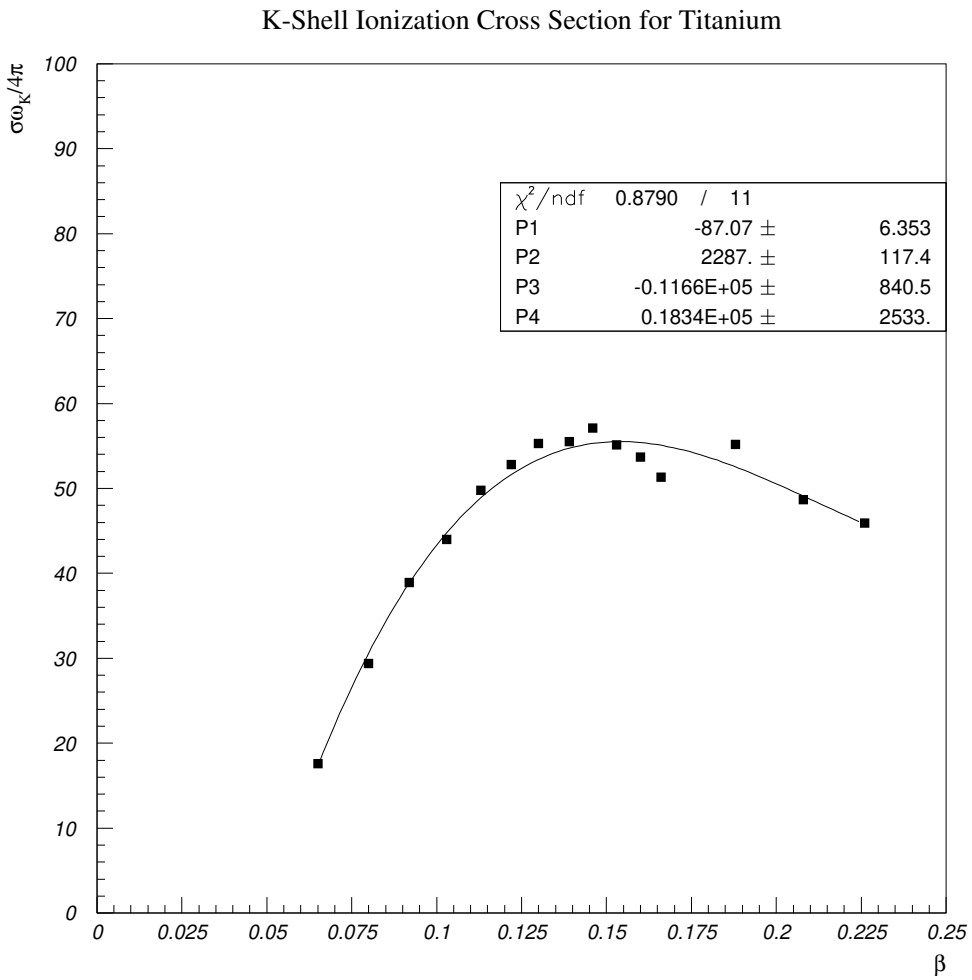

Figure 15: The K-shell ionization cross section as a function of incident particle velocity for titanium. Data points from reference 2. Note that the cross section is scaled.

We therefore created a Monte Carlo simulation of the target geometry and the basic photoelectric processes which dominate the interactions below 100 keV. The foil measurements became cross-checks of the Monte Carlo, which was then used to make estimates for the excitation from a realistic background and from kaons.

We believe that entrance foils will be necessary to help shield the CCDs from direct background X rays. We therefore considered a geometry in which a 25 micron zirconium foil beneath a 75 micron titanium foil would be placed above the isolation vacuum entrance window, and alternating 50 micron titanium and zirconium foils would cover the target walls. The Monte Carlo results for such a geometry are summarized in table 9.

Thus, the ratio of titanium to zirconium K_α X rays for this configuration is about 3:1. The optimum Ti/Zr intensity ratio for the calibration peaks was shown to be 11:1. However, this value is for the case of no background, and if there is some background, which is the case we will be faced in the actual experiment, the ratio should be smaller (more zirconium X rays.)

In any case, as long as we have enough titanium X rays, it does not matter if there are extra zirconium X rays. Keep in mind that at a luminosity of 10^{32} cm^{-2} s^{-1} we expect a maximum of 400 kaonic hydrogen K_α X rays per day (assuming a yield of 3%). Thus, the expected ratio of titanium K_α X rays to kaonic hydrogen K_α X rays is at least 1.6:1. With such a ratio, the systematic error on the energy calibration will always be limited by the statistics of the kaonic hydrogen peak. We therefore believe that our simulated geometry is a good starting point for the actual kaonic hydrogen measurement.

References

[1] M. C. Lépy, *et.al.*, Nucl. Inst. Meth. **A 353** (1994) 10

[2] G. A. Bissinger, *et.al.*, Phys. Rev. A **1** (1970) 841

[3] J.D. Garcia, *et.al.*, Rev. Mod. Phys. **45** (1973) 111

[4] E. Browne and R.B. Firestone, *Table of Radioactive Isotopes*, John Wiley and Sons.

Table 2: Conditions under which the measurements were performed. Measurement 5 was done with both the titanium and zirconium foil at the bottom and the titanium foil was on top of the zirconium foil. Measurement 6 was similar but this time the zirconium foil was on top of the titanium foil. For measurements 1-6, the bottom foil was placed at position 1, and for measurements 8, the bottom foil was placed at position 2. For measurements 7 and 8, two corners of the inner wall of the target cell were covered with titanium foils and the other two with zirconium foils (see figure 1).

No.	Ti foil (50 μm)	Zr foil (50 μm)	Exposure time (min)	CCDs
1	Side	—	590	A-D
2	—	Side	1340	A-D
3	Side	Bottom	1195	A-D
4	Bottom	Side	1230	A-D
5	Bottom (top)	Bottom (bottom)	901	A-D
6	Bottom (bottom)	Bottom (top)	970	A-D
7	Side	Side	500	A-H
8	Side and Bottom	Side	630	A-H

Table 3: Number of counts observed in each peak. The symbol "—" indicates either that X rays corresponding to that line were not observed or that the quality of the data was not good enough to be quoted (e.g. the peak was too close to the edge of the spectrum).

No.	Ti K_α (counts/min/half-CCD)		Zr K_α (counts/min/half-CCD)	
	CCD A/B/C/D	Average	CCD A/B/C/D	Average
1	1.46/1.07/1.42/1.10	1.26		
2			—/0.26/0.26/0.14	0.22
3	0.66/0.50/0.71/0.67	0.64	0.31/—/0.22/—	0.27
4	1.26/1.06/1.13/1.10	1.14	0.098/0.14/0.15/0.075	0.12
5	0.59/0.61/0.54/0.54	0.57	0.210/0.090/0.147/0.190	0.16
6	—/—/—/—	—	—/0.37/0.60/0.33	0.43
7		0.76		0.12
8		0.52		0.11

Table 4: Number of counts observed in each peak (average over all the CCDs used). The symbol "—" indicates either that X rays corresponding to that line were not observed or that the quality of the data was not good enough to be quoted (e.g. the peak was too close to the edge of the spectrum).

No.	Ti foil	Zr foil	Ti K_α counts (/min/half-CCD)	Zr K_α counts (/min/half-CCD)
1	Side		1.26	
2		Side		0.22
3	Side	Bottom	0.64	0.27
4	Bottom	Side	1.14	0.12
5	Bottom (top)	Bottom (bottom)	0.57	0.16
6	Bottom (bottom)	Bottom (top)	—	0.43
7	Side	Side	0.76	0.12
8	Side and Bottom	Side	0.52	0.11

Table 5: Monte Carlo counts observed in each peak. The symbol "—" indicates that X rays corresponding to that line were not observed.

No.	Ti foil	Zr foil	Ti K_α counts (/min/half-CCD)	Zr K_α counts (/min/half-CCD)
1	Side	—	1.66	—
2	—	Side	—	0.27
3	Side	Bottom	0.80	0.54
4	Bottom	Side	1.85	0.23
5	Bottom (top)	Bottom (bottom)	1.06	0.17
6	Bottom (bottom)	Bottom (top)	—	0.50
7	Side	Side	0.86	0.17
8	Side and Bottom	Side	0.48	0.10

Table 6: Number of counts observed using the online single-pixel analysis with various cuts.

cut conditions	Ti K_α counts (Gaussian fit)	Zr K_α counts (channels 850-920)
1 σ	609	114
1.5 σ	1140	250
2 σ	1442	366
above, plus MaxValE(Nbr): 8-14	1540	538
above, plus StandDevE(Nbr): 8-14	1585	627

Table 7: Attenuation length of X rays of relevant energies in various material.

X-ray energy (keV)	Attenuation length (μm) titanium	zirconium	mylar
4.5	20.1	2.5	188
13.9	49.6	50.8	5210
15.8	71.1	71.9	7250
17.5	95.6	95.5	9310
22.0	183	27.2	15000
59.5	2820	402	38400

Table 8: X-ray intensity per 100-K shell vacancies

X ray	titanium	zirconium
$K_{\alpha 1}$	12.8	41.0
$K_{\alpha 2}$	6.4	21.4
$K_{\beta 1}$	1.4	6.2
$K_{\beta 2}$	—	1.3
$K_{\beta 3}$	0.7	3.2

Table 9: The foil Monte Carlo prediction of the total rates of K_α calibration X rays.

Source	Foil Position	Ti K_α /day	Zr K_α /day
Background	entrance	275	140
Photons	wall	25	75
Kaons	entrance	255	—
	wall	85	—
	TOTAL:	640	215